Impact of positive charge and ring-size on the interactions of calixarenes with DNA, RNA and nucleotides

Ivona Krošl, Ena Otković, Ivana Nikšić-Franjić, Benoît Colasson, Olivia Reinaud, Aleksandar Višnjevac, Ivo Piantanida

NJC

PAPER

Impact of positive charge and ring-size on interactions of calixarenes with DNA, RNA and nucleotides

Received 00th January 20xx,
Accepted 00th January 20xx

DOI: 10.1039/x0xx00000x

www.rsc.org/

Ivona Krošl[a],† Ena Otković[a],† Ivana Nikšić-Franjić[a], Benoit Colasson[b], Olivia Reinaud[b], Aleksandar Višnjevac[a], and Ivo Piantanida[a,*]

Comparison of neutral and cationic calix[6]arene and calix[4]arene derivatives revealed that only cationic analogues non-covalently bind to ds-DNA and ds-RNA, by insertion into DNA minor groove or RNA major groove. Also, cationic analogues revealed strong and highly selective charge-dependent stabilization of AT-DNA against thermal denaturation, calix[6]arene trication being for an order of magnitude more efficient than its calix[4]arene dicationic analogue. At variance to DNA/RNA selectivity for only cationic calixarenes, both, neutral and cationic calixarenes bind nucleoside monophosphates with similar efficiency, by forming tweezer-like supramolecular complexes, with nucleobases inserted between aromatic pendant arms grafted to calixarene rims. Such nucleotide-calixarene complexes were monitored by emission change of calixarene as a function of nucleobase insertion, whereas calixarene was inserted into DNA/RNA polynucleotide groove with no change in the calixarene emission – stressing importance of the ligand insertion within calix-basket for the fluorimetric sensing.

Introduction

Synthetic small molecules targeting DNA/RNA or nucleotides have attracted considerable interest due to a huge versatility in biochemical and biomedical applications, spanning from drugs-like to toxic properties, or as various probes for monitoring of bio-related processes.[1,2] The research on DNA/RNA-interacting small molecules has been mostly focused on its impact on the DNA/RNA function or selective/specific DNA/RNA labelling.[2-4] However, huge complexity of DNA- or RNA- coded processes, which do not depend only on coding DNA base pair sequences, but also include epigenetics, has only recently attracted more attention.[5,6]

Calixarenes were traditionally studied as supramolecular receptors for various low molecular weight cationic, anionic or neutral species, but only marginally investigated for their biological effects or applications.[3,4] However, systematic study revealed that cationic calixarenes can be applied as innovative DNA-transfection agents.[5,6] Also, in our previous report we demonstrated that particular cationic calixarene-dimers bind into ds-DNA major groove,[7] which is a rather rare propensity of small molecules that commonly target DNA minor groove.[2] Other studies with monomeric calixarenes revealed intriguing bioactivity, and different DNA-binding profile, which was, at the time, not studied in detail.[7]

[a] *Institut Ruđer Bošković, Bijenička c. 54, 10000 Zagreb, Croatia*
[b] *Université de Paris - Laboratoire de Chimie et Biochimie Pharmacologiques et Toxicologiques, CNRS UMR 8601, 45 rue des Saints Pères, 75006 Paris, France*
* *Correspondence: pianta@irb.hr (I.P.); Tel.: +385-1-4571-326*
† I.K. and E.O. share the first authorship for equal contribution.
Electronic Supplementary Information (ESI) available: [details of any supplementary information available should be included here]. See DOI: 10.1039/x0xx00000x

Within the last decade we have developed three generations of calix[6]arene-based (funnel), as well as two generations of resorcinarene-based (bowl) supramolecular systems featuring two, three or four methylimidazole-containing coordination arms grafted at the large rim, and with ever increasing level of biomimicry.[8-10] Major breakthrough in development of fully biomimetic systems has been achieved recently with the optimized synthetic procedure for water-soluble structures, which are now readily available.[11-13] Cationic calix[4]arene **2** and calix[6]arene **4** (Scheme 1) studied within this report were among the first examples of our water soluble systems, at the time showing promising recognition of metal cations and primary amines in aqueous solution.[14,15]

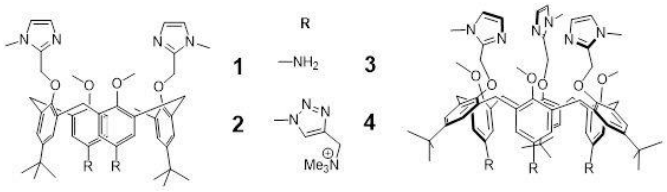

Scheme 1. Molecular structures of studied cationic calixarenes **2** (as a chloride salt), **4** (as a nitrate salt) and their non-charged analogues **1** and **3.**

Previously published calixarene derivatives targeting DNA, based their action on the substituents bearing multiple positive charges, which strongly interacted with DNA negatively charged backbone, in several cases strongly condensing plasmid-DNA into globular species followed by efficient DNA-transfection into the cells,[5,6] while dimeric derivatives did not cause DNA-condensation but were instead inserted into the DNA major groove.[7] In contrast to previously published results, in this work we focused on calixarenes with very short, triazole-attached

permethylated positively charged substituents (**2** and **4**) and their neutral analogues (**1** and **3**). We were particularly intrigued by the possible influence of several structural features of these calixarenes on the non-covalent interactions with double stranded DNA or RNA, as well as with nucleotides as building blocks of nucleic acids. Based on our previous work[7] we presumed minor groove binding as the mode of interaction with ds-DNA, which should be controlled by the size (**1**, **2** *vs*. **3**, **4**) and charge (**1**, **3** *vs*. **2**, **4**) of the calixarenes. Moreover, ds-RNA major groove could be another suitable binding site, thus fine structural differences between **1**, **2**, **3** and **4** could lead to ds-DNA *vs*. ds-RNA selectivity. Furthermore, **1**-**4** with several aromatic substituents grafted to one calixarene rim (**1**, **3**) or both rims (**2**, **4**) resemble to some extent to supramolecular tweezer-like constructs designed to bind nucleotides, which by fine interplay of electrostatic, hydrophobic, aromatic stacking and H-bonding interactions demonstrated particular selectivity towards various nucleotides.[16-19]

Results and discussion

Characterization of Studied Compounds in Aqueous Solutions

Studied compounds are moderately soluble in water as described earlier.[14,15] However, for easier handling, stock solutions were prepared in DMSO at 5 mM concentrations, stored in a refrigerator and diluted in buffer prior to use.

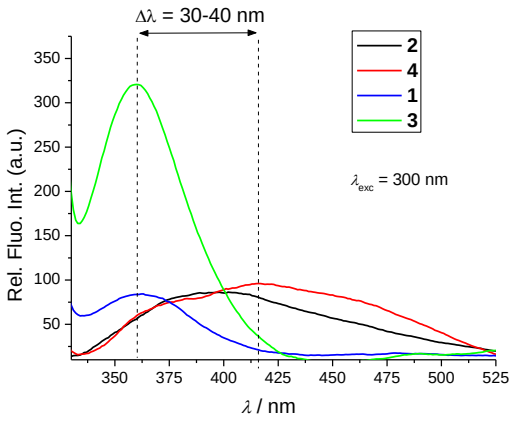

Figure 1. a) The fluorescence spectra of **1**-**4** (c = 2 × 10^{-6} M), λ_{exc} = 300 nm, at pH 7.0, sodium cacodylate buffer, I = 0.05 M.

The UV/Vis spectra in buffered solution at pH 7.0 revealed that all compounds have absorption maxima < 300 nm, with a shoulder at λ = 300 nm, and hence are convenient for spectrophotometric studies of interactions with ds-DNA/RNA (absorbing below 300 nm). Absorbancies for all compounds were proportional to their concentrations up to 10 µM.

Literature search on related calixarene analogues did not show any mention of their fluorescence emission. However, 1,2,3-triazole-phenol based ''turn-on'' fluorescence sensor for the detection of anions[20,21] resembles closely to the building block used in **2** and **4**. This prompted us to check the fluorescence emission properties of **1**-**4**. Upon excitation at different absorption maxima or at absorption shoulder at 300 nm (chosen for convenience of not overlapping with the absorbance of DNA), studied compounds exhibited very weak but applicable fluorescence (Figure 1), with the intensity proportional to compounds concentration up to 5 µM. The collected excitation spectra were in accordance with UV/Vis spectra, supporting that the same chromophore is responsible for absorption and emission of the light.

Relative quantum yields, determined in comparison to NATA standard (*N*-acetyl-L-tryptophanamide, Φ_R=0.14, λ_{exc} = 280 nm; λ_{em} = 300 – 360 nm) were very low (ESI, Table S2; Φ_f < 0.005), mutual comparison generally confirming order of magnitude lower Φ_f values for triazole-analogues **2**, **4** in respect to amine – derivatives **1** and **3**. In order to check whether studied compounds have stable, unique excited state, we performed three experiments by using three different excitation wavelengths (270, 280 and 290 nm) and for each wavelength the same quantum yield was obtained.

Comparison of emission maxima revealed that neutral molecules **1** and **3** emit light at about 30 - 40 nm shorter wavelength in comparison to their triazole-cationic analogues **2** and **4**. To address this by computational chemistry methods, the fluorescence spectra of compounds **1** and **2** were calculated (ESI, Fig. S6) to identify the part of the molecule responsible for the fluorescence, as well as the type of molecular orbitals dominating the transitions. The structures of **1** and **2** were optimized employing the density functional theory in conjunction with the polarizable continuum model (DFT-D3/PCM) for a fully implicit description of the aqueous environment. The global hybrid B3LYP exchange-correlation functional was used for geometry optimizations in ground and first excited states, as well as for harmonic frequencies calculations. The dispersion corrections where included using the Grimme's D3 model.[22] The structures where optimized using the 6-31G(d), since this level of theory showed very good performance in previous studies of fluorescent calix[4]arenes.[23] The fluorescent spectra were calculated employing the time dependent density functional theory (TD-DFT/B3LYP/6-31G (d)) with corrected linear response approach. All calculations were done in Gaussian16 program package.[24] According to the calculations, approximately the same red-shift (for 47 nm) in emission wavelength was observed in case of compound **2** in comparison with **1**. The emission of **1** and **2** originates from the transition of electrons in their HOMO (π orbital) to LUMO (π orbital, Fig. 2.) according to the 100 % ratios, showing the obvious $\pi^* \rightarrow \pi$ characters, the electron-donating HOMO of **1** π distributed mainly on benzene ring and amino group and the electron-accepting LUMO is also a π orbital but distributed on two adjacent benzene rings.[25] The results obtained for calixarene **2** showed a charge transfer from *tert*-butyl benzene ring to benzene-triazole subunit. As shown in theoretical calculations, the energy difference between HOMO and LUMO of compound **2** is lower than of compound **1** so the compound **2** has red-shifted emission wavelength,[26] in accordance with obtained experimental results (Figure 1). It is expected that calix[6]arenes **3** and **4** with larger ring size will be more flexible than calix[4]arenes **1** and **2**, and due to more fluorophores, exhibit increased emission intensity.

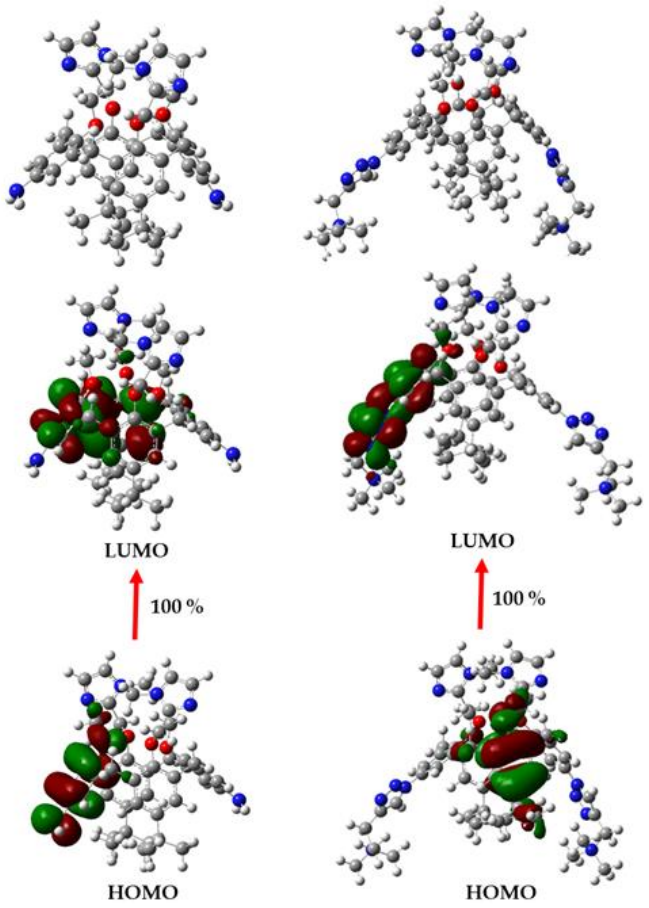

Figure 2. The excited states optimized structures of calix[4]arene **1** (left) and **2** (right) and the emission mechanism predicted by TD-DFT.

Interactions with nucleotides

Taking advantage of the weak fluorescence exhibited by **1**-**4**, we performed fluorimetric titrations by adding nucleotide aliquots to buffered solutions of **1**-**4** and measuring resulting emission alteration. In all cases, addition of nucleotide caused fluorescence quenching (Figure 3, ESI, Fig. S7); however, intensity of emission change and binding constant calculated for 1:1 stoichiometry of complex formed, depended strongly on which nucleotide and calixarene were involved (Table 1). Fitting data to other stoichiometries (2:1 or 1:2) by Specfit program[27,28] for multivariate analysis, did not give better fit or logical species distribution.

Due to the generally weak emission of the calixarenes, titration data points show some variation and thus values of binding constants obtained by fitting procedures are accurate within the order of magnitude, consequently only differences larger than the order of magnitude can be considered as significant. Analysis of binding constants (log K_s, Table 1) revealed that neutral compounds **1** and **3** show similar affinity for nucleotides as compared to their cationic analogues **2** and **4**, which leads to the conclusion that electrostatic interactions between positive and negative charges did not contribute significantly. Furthermore, only neutral compounds **1** and **3** exhibited similar affinity toward purine (A, G) and pyrimidine (U, C) bases, while cationic **2** and **4** bind purine (A, G) more than an order of magnitude stronger than pyrimidine (U, C) bases. The diameter of the calixarene cavity in the studies compounds does not allow the deep inclusion of nucleobases inside the calixarene cavity, but the flexibility and spacing of aromatic subunits at both calixarenes rims (Fig. 4) allow for a possible insertion of aromatic ligands (such as nucleobases) in the form of a supramolecular tweezer-like complex.

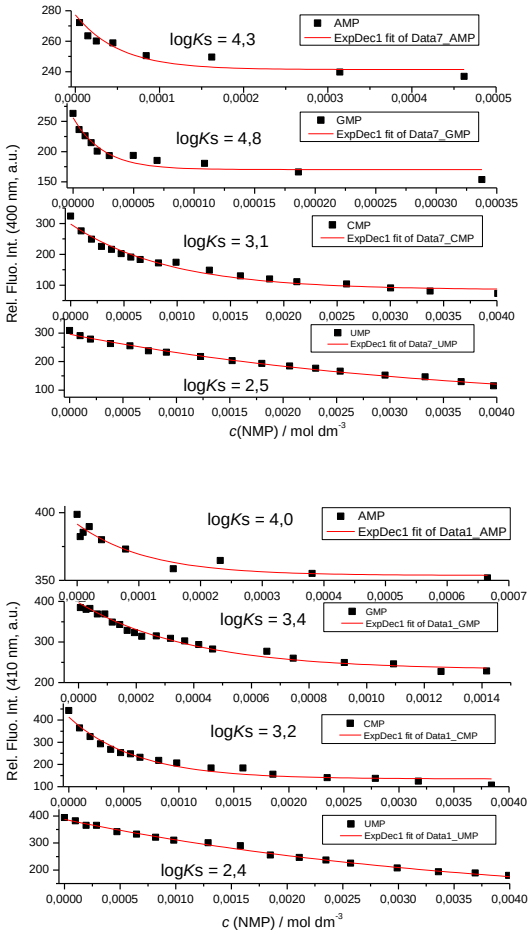

Figure 3. Changes in fluorescence of: UP) **2** (λ_{exc} = 300 nm, λ_{em} = 400 nm, $c = 1 \times 10^{-6}$ M) or DOWN) **4** (λ_{exc} = 300 nm, λ_{em} = 400 nm, $c = 1 \times 10^{-5}$ M); upon addition of various mononucleotides. Done at pH 7.0; sodium cacodylate buffer, I = 0.05 M.

Binding constant values (log K_s) > 4 do support formation of the tweezer-like type of nucleobase-calixarene complex, where the nucleobase is inserted between two or three imidazole or triazole subunits, based on the sandwich-type aromatic stacking interactions (Fig. 4). Similar tweezer-like complex with a nucleobase inserted between aromatic subunits has been characterized previously.[18,19] Taking into account the structures of the studied calixarenes, for neutral analogues of **1** and **3**, the nucleobase binding site would be between imidazole subunits, whereas for cationic analogues **2** and **4**, there is an additional possibility of binding between triazole-cation subunits – allowing additional electrostatic interactions between negatively charged phosphate of the nucleotide and cationic part of **2** and **4**.

Table 1. Binding constants log K_s[a] and emission quenching efficiency of complexes ([b]ΔInt) of **1**-**4** with nucleotides calculated by processing fluorimetric titrations (c = 2 × 10^{-6} M), at pH = 7.0, sodium cacodylate buffer, I = 0.05 M.

	AMP	GMP	UMP	CMP
2	4.3±0.1 (ΔInt = 0.8)	4.8±0.2 (ΔInt = 0.6)	2.5±0.3 (ΔInt = 0.3)	3.1±0.3 (ΔInt = 0.4)
4	4.0±0.1 (ΔInt = 0.9)	3.4±0.3 (ΔInt = 0.6)	2.4±0.3 (ΔInt = 0.4)	3.2±0.2 (ΔInt = 0.2)
1	5.0±0.1 (ΔInt = 0.8)	4.7±0.1 (ΔInt = 0.8)	4.1±0.2 (ΔInt = 0.6)	[c]NP
3	4. ±0.1 (ΔInt = 0.6)	5.0±0.1 (ΔInt = 0.5)	5.0±0.1 (ΔInt = 0.6)	4.7±0.2 (ΔInt = 0.6)

[a] Obtained by processing titration data by the nonlinear regression fitting method (Origin 7.0) according to the model the compound / NMP = 1: 1 stoichiometry complex; correlation coef. R>0.99.

[b] ΔInt = Int (100% complex) / Int0;

[c]NP = too small emission changes for reliable data processing

The addition of a nucleotide to any calixarene generally quenches its fluorescence (Figure 3), likely due to the partial aromatic π-π interactions between the nucleobase and the fluorophore, occuring during the insertion of part of the nucleotide between the calixarene arms. It is well known that such π-π interactions facilitate non-radiative relaxation of the fluorophore, but they are often not 100 % effective, leading to only a partial quenching of the emission. Further, a detailed analysis of the emission quenching efficiency (Table 2, ΔInt) showed some selectivity. The main structural difference between the tested calixarenes is that compounds **2** and **4** contain two and three positive charges, respectively, while the compounds **1** and **3** are neutral. Purine bases induce similar emission quenching of charged or neutral analogues, but a significant selectivity is observed with pyrimidine bases (C and U), which are generally smaller in size than purine bases (A and G). Only for cationic calixarenes (**2** and **4**), the addition of any pyrimidine base resulted in significantly stronger fluorescence quenching (ΔInt) as compared to purine bases. Very likely, a smaller pyrimidine base penetrates deeper into the calixarene structure, thus influencing its fluorescence properties more strongly.

To confirm this assumption we investigated, by set of computational methods the possibility of inclusion of both pyrimidine and purine nucleobases, specifically CMP and AMP into the positively charged calixarene **4** cavity. Two complexes of calixarene **4** with each mononucleotide were prepared, one with mononucleotide oriented between the imidazole groups (Fig. 4. left) and the other between triazole subunits (Fig. 4. right). The molecular dynamics simulations were done for 50 ps with a time step of 4 fs at the temperature of 298.15 K, which was found sufficient to reach the most stable thermodynamic state. The water was modelled implicitly with generalized Born model with surface area (gbsa).

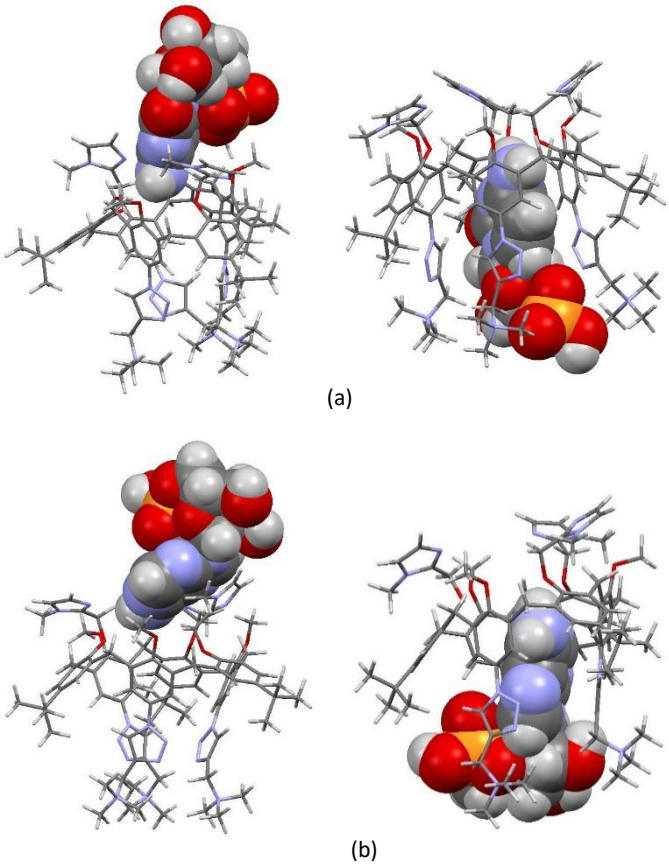

Figure 4. Optimized complexes of calixarene **4** (capped sticks style) with nucleotides (space fill) inserted between imidazoles (left) and triazoles (right): a) CMP, b) AMP. Determined by semiempirical GFN2-xTB method and molecular dynamics simulations

The most stable structures of the complexes are shown on Fig. 4, demonstrating that for cationic derivative **4**, nucleobase insertion from both, imidazole or triazole, side is indeed possible. Complexes are stabilized with aromatic stacking interactions between nucleobase and aromatic substituents of calixarene, while for triazole side negatively charged phosphate groups are oriented towards positively charged trimethylamine group in triazole binding subunit, suggesting electrostatic interaction contribution. It is important to note that CMP enters a cavity more deeply in comparison to AMP (Fig.4 right; a) and b)), supporting aforesaid impact on emissive properties of fluorophores and consequent stronger emission quenching in comparison to purine nucleotides.

Interactions with ds-DNA, ds-RNA

The choice of ds-DNA and ds-RNA in this study was driven by significant differences in the secondary structure of particular homogeneous polynucleotide sequences (for detailed structural features, see ESI, Table S1): poly dAdT - poly dAdT are characterized by typical B-helical structure and minor groove ideal for small molecule binding; poly dGdC - poly dGdC minor groove is sterically blocked by guanine amino groups significantly hampering small molecule insertion; poly A — poly U presenting typical RNA A-helical structure with a major groove as a potential target for small

molecules. Also, for comparison, we used naturally isolated DNA from calf thymus (ct-DNA), characterized by a typical B-helical structure and an equal amount of AT- and GC-base pairs. All chosen polynucleotides are 100–200 base pairs long, ensuring a large quantity of identical, mutually independent binding sites for a small molecule and thus rendering the contribution of molecule binding at polynucleotide termini negligible.

Thermal denaturation experiments

The thermal denaturation experiments provide information about the ds- polynucleotide helix thermal stability as a function of interaction with added small molecules.[29] The difference between the T_m value of free ds-polynucleotide and a complex with a small molecule (ΔT_m value) is an important factor in the characterization of small molecule/ds-polynucleotide interactions. Thermal denaturation is particularly informative for presumed polynucleotide groove binding of small molecules, like hereby studied calixarenes. Namely, insertion into polynucleotide groove is controlled by several steric factors: groove width, groove depth and particularly by steric obstruction of guanine amino groups in the DNA minor groove, which effectively hamper efficient binding in GC-sequences. For instance, all typical DNA minor groove binders are highly selective or even specific for AT-sequences.[2] Moreover, thermal denaturation of DNA/RNA is also sensitive to electrostatic interactions of positively charged small molecules with negatively charged DNA/RNA backbone.[30]

Table 2. ΔT_m values[a] (°C) for ratio [b]r = 0.3 of **1** - **4** added to various polynucleotides

	ct-DNA	pApU	p(dAdT)$_2$	pdA - pdT
1	0	0	0	0
2	0	2	1	1
3	0	0	0	0
4	0	1	10	3

[a] ΔT_m-Value error ± 0.5 °C; [b] r = (compound)/(polynucleotide).

Addition of **1**-**4** to studied DNA/RNA resulted in quite selective stabilization of double stranded AT(U) containing polynucleotides (Table 2, ESI, Figs S18-S25). The impact of neutral calixarenes **1** and **3** on stabilization of ds-polynucleotides was negligible for all studied DNA/RNA (Table 2), strongly stressing the importance of positive charge for effective binding to DNA/RNA. Cationic analogues **2** and **4** selectively stabilized AT(U) polynucleotides, whereas mixed sequence ct-DNA, containing 42 % of GC-base pairs, was not stabilized which suggests that grooves are dominant binding sites. Smaller, +2 charged calixarene **2** similarly stabilized all AT(U)-polynucleotides, while larger +3 charged calixarene **4** much stronger stabilized p(dAdT)$_2$ with groove width of 6.3 Å, than polynucleotides with narrower grooves [pApU (3.8 Å) or pdA – pdT (3.3 Å)].

Fluorimetric titrations

The emission of studied **1**-**4** changed only negligibly upon addition of any ds-DNA or ds-RNA, which is in compliance with location of presumed fluorophores inside calixarene ring (phenol-triazole or phenol-amine units). Such fluorophore would be sensitive to bound cations or deeply inserted nucleobases, but structure of DNA/RNA binding sites does not include insertion into calixarene but rather more likely enveloping calixarene inside DNA/RNA.

In order to mitigate the low emission responsiveness of calixarenes upon binding to ds-DNA/RNA, we opted for Indicator Displacement Assay (IDA) methodology,[31] particularly for ethidium bromide (EtBr) displacement assay by preparing a highly emissive EtBr/polynucleotide complex and then displacing EtBr by addition of calixarene, monitoring simultaneously the decrease of EtBr emission (Figure 5, ESI, Figs S8-S17).[32,33]

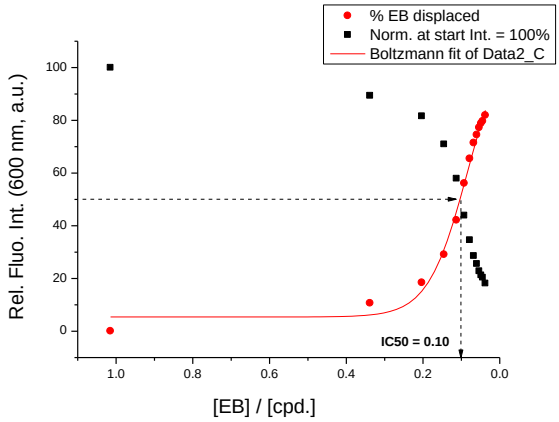

(a)

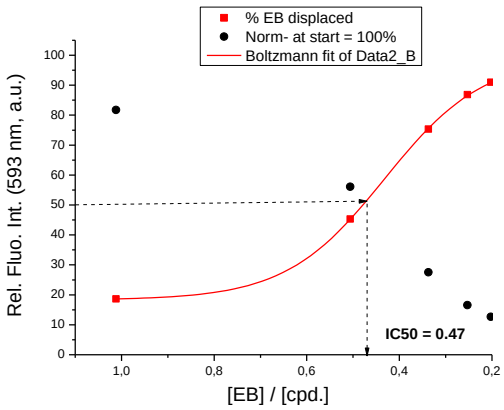

(b)

Figure 5. Changes in fluorescence of ethidium bromide (c = 5 × 10^{-6} M, λ_{exc} = 505 nm, λ_{em} = 600 nm) from the complex with the p(dAdT)$_2$ (c = 5 × 10^{-5} M): a) upon addition of **2** or b) upon addition of **4**. Note five times larger quantity of **2** in comparison to **4**, necessary to reach IDA50%. Done at pH 7.0; sodium cacodylate buffer, I = 0.05 M.

Table 3. The IDA50% ratios of ethidium bromide against calixarenes **1** – **4** (IDA50% = [EtBr] / [calixarene] at which 50% of EtBr is displaced) obtained by displacement of ethidium bromide ($c = 5 \times 10^{-6}$ M) from the complex with the tested polynucleotide ($c = 5 \times 10^{-5}$ M). Measurements were performed at pH = 7.0; sodium cacodylate buffer, $I = 0.05$ M.

	ctDNA	$p(dAdT)_2$	$p(dGdC)_2$	pApU
1	b	b	b	B
2	0.15	0.10	0.11	0.09
3	b	b	b	b
4	0.34	0.47	0.68	0.68

[a] The IDA50% value is calculated as a ratio [EtBr] / [calixarene] = (Int(EtBr-DNA complex) – Int(EtBr)) / 2 ; [b] Negligible change of Int(EtBr-DNA complex) prevented calculation of IDA50% value.

Calculated IDA50% (Indicator Displacement Assay) values (Table 3) corroborated the previously established dependence of the binding to a polynucleotide chain and positive charge of a binder (*vide supra*). +3 charged **4** is 3 - 6 times more effective in EtBr displacement as compared to +2 charged **2**, while neutral analogues **1** and **3** were unable to displace EtBr from any ds-DNA/RNA. Since ethidium bromide is actually an intercalator, which is displaced from DNA/RNA by groove binding calixarenes **2** and **4**, one cannot directly derive apparent binding constant from calculated IDA50% values (Table 3). However, displacement took place close to an equimolar ratio of EtBr and **4**, suggesting roughly comparable affinity. Therefore, in order to verify these IDA50% values, we performed competition experiments with DAPI, a typical minor groove binder, highly selective to AT-DNA minor groove, and for monitoring displacement we opted for circular dichroism as a fluorescence-independent method (see below).

Circular dichroism experiments

To study in more detail the structural properties of the formed complexes, we used circular dichroism (CD) spectrophotometry.[34] A small molecule can, upon binding to polynucleotides, acquire an induced (I)CD signal, positioned at the absorption bands of the small molecule, in the case of our compounds **1**-**4** in the range 300 – 550 nm, not coinciding with the DNA/RNA CD signals. The character and the magnitude of the ICD signal offer valuable information for the determination of binding modes (intercalation, agglomeration, groove binding, etc.).[35] Minor groove binding to ds-DNA orientates the ligand approximately at 45° with respect to the DNA chiral axis, giving a strong positive ICD band. Intercalation brings the aromatic moiety of the ligand in a coplanar arrangement with the base pairs, giving only a weak ICD band (in the majority of cases with a negative sign due to parallel orientation of the transition vector of the ligand and the longer axis of the surrounding base pairs).[34,35]

Studied calixarenes are achiral, thus do not possess intrinsic CD spectra. Addition of any studied calixarene to any DNA or RNA did not change significantly the CD spectrum of a polynucleotide and no induced CD bands at > 300 nm were observed (ESI, Fig. S26, S27). Considering the barrel-like shape of calixarene molecules, it is very likely that transition moments of their absorption spectra did not align uniformly in respect to the DNA/RNA chiral axis (thus no ICD bands) and that their insertion into DNA/RNA grooves did not disturb significantly the DNA/RNA helicity.

However, in order to confirm a presumed binding of cationic calixarenes **2** and **4** in the DNA minor groove, we performed series of displacement experiments with DAPI, a well-known minor groove binder. DAPI binds into AT-DNA minor groove with high affinity, yielding strong positive ICD band at about 375 nm.[36] If cationic calixarenes bind also into DNA minor groove, they should efficiently displace DAPI, but if they bind into major groove, DAPI ICD band should remain unchanged.[7] Indeed, addition of **2** or **4** very efficiently displaced DAPI, as monitored by disappearance of DAPI ICD band (Figure 6, ESI, Figs. S28, S29). Observed IDA50% values differ by factor of four, suggesting that smaller **2** displaces DAPI from the AT-DNA minor groove somewhat more efficiently than its larger analogue **4**. Intriguingly, difference in IDA50% values for the ethidium bromide displacement (Table 3) was opposite, likely due to the different binding modes of ethidium (DNA intercalator) and DAPI (DNA minor groove binder).

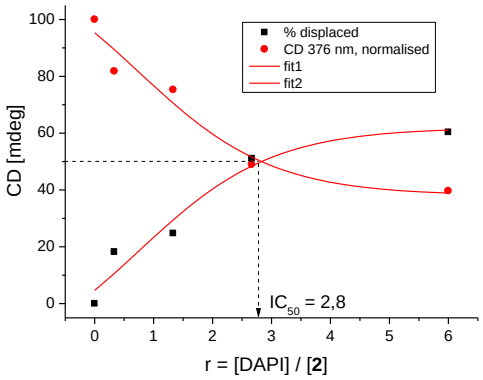

(a)

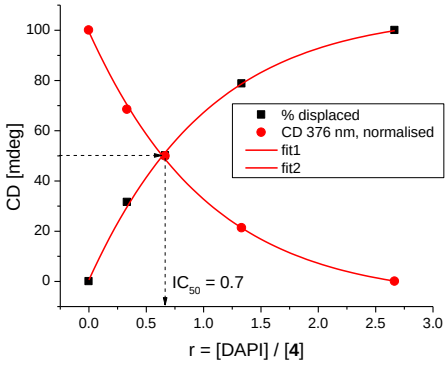

(b)

Figure 6. Changes in induced CD band of DAPI at 375 nm ($c = 5 \times 10^{-6}$ M) from the complex with the $p(dAdT)_2$ ($c = 2 \times 10^{-5}$ M): a) upon addition of **2** or b) upon addition of **4**. Done at pH 7.0, buffer sodium cacodylate, $I = 0.05$ M.

Conclusions

At variance to previously reported evidences for hereby studied class of calixarenes, we have demonstrated that they do emit weak but applicable fluorescence, responsive for inclusion-type of complexes. We also identified phenol-amine and phenol-triazole subunits as responsible for the fluorescence of our compounds.

Studied series of neutral and cationic calixarenes demonstrated two different modes of interaction with biorelevant targets. The mononucleotides (NMP) form tweezer-like complexes with their nucleobases inserted between aryl-substituents grafted to calixarene rim, dominantly based on aromatic stacking and hydrophobic interactions – as evidenced by similar affinity of neutral and cationic calixarenes. Formation of such complexes is easily monitored by change of calixarene fluorescence, particularly of cationic calixarenes which reveal selective response to pyrimidine bases (UMP, CMP).

Unlike the small molecule (NMP) complexation, only cationic analogues **2** and **4** of hereby studied calixarene derivatives bind to large polynucleotides by insertion into a DNA minor and RNA groove. The binding interactions involved in the formation of the resulting assemblies have an important electrostatic contribution, since only cationic calixarenes **2** and **4** show measurable interactions. Nevertheless, the efficiency of EtBr displacement by far exceeds the effect of only two or three positive charges per calixarene molecule, thus suggesting that also hydrophobic interactions are involved (based on water expulsion from a DNA/RNA groove). This hydrophobic effect is corroborated by efficient displacement of DAPI from AT-DNA groove. CD experiments showed that the insertion of calixarene into DNA or RNA grooves does not disturb the secondary structure of the double helix significantly; however more efficient DAPI displacement by derivative **2** in comparison to its larger analogue **4** does reveal a limited steric-controlled selectivity.

The existence of two different possible modes of binding open an avenue for an innovative simultaneous monitoring system, in which mixture of mononucleotides and large polynucleotides could be simultaneously tested for both components: the calixarene emission change would be a qualitative mark for the formation of a complex between the calixarene and a mononucleotide, while efficient displacement of EtBr from DNA and/or selective AT-DNA stabilization would signal calixarene binding to a polynucleotide chain. The calix[6]arenes **3** and **4** herein studied are by their design rather flexible and their flexibility (this especially stands for **4**) might also be an important factor to modulate to gain more information about the DNA/RNA binding of this class of molecules. This work is currently in progress in our laboratories.

Experimental section

General information

Compounds **1**-**4** were prepared and characterized as described earlier.[14,15,37]

Computational methods

For calixarene spectrophotometric properties modelling the global hybrid B3LYP exchange-correlation functional was used for geometry optimizations in ground and first excited state, as well as for harmonic frequencies calculations. The dispersion corrections where included using the Grimme's D3 model.[38] The structures where initially optimized using the Pople-style basis set (3-21G) and reoptimized using the 6-31G(d) since this level of theory showed very good performance in previous studies of fluorescent calix[4]arenes.[39] The fluorescent spectra where calculated employing the time dependent density functional theory (TD-DFT/B3LYP/6-31G (d)) with corrected linear response approach. All calculations were done in Gaussian16 program package.[24]

For modelling calixarene/nucleotide complexes we employed semiemipirical tight-binding GFN2-xTB method[40,41] for optimizations and molecular dynamics to explore the conformational space and noncovalent interactions. Grimme's xtb (Semiempirical Extended Tight-Binding Program Package)[42] program was used for geometry optimizations and molecular dynamics simulations as well. Calixarene 4 was initially optimized in Gaussian16 at the PCM-B3LYP-D3/G-31G(d) level of theory. 3D preliminary structures of AMP and CMP were taken from ChemSpider website[43] in form with deprotonated phosphate group to ensure the experimental conditions in neutral buffered solutions.

Study of Interactions with nucleotides and ds-DNA/RNA

All measurements were performed in aqueous buffer solution (pH = 7.0, sodium cacodylate buffer, I = 0.05 M). The UV-Vis spectra were recorded on a Varian Cary 100 Bio spectrometer, fluorescence spectra were recorded on a Varian Cary Eclipse fluorimeter, and CD spectra were recorded on JASCO J815 spectropolarimeter at 25.0 °C using appropriate quartz cuvettes (path length:1 cm).

Nucleotides (AMP, GMP, UMP and CMP) were purchased from Sigma, dissolved in stock solutions of c = 0.01 M and used. Polynucleotides were purchased as noted: poly dAdT–poly dAdT, poly A–poly U, poly dA – poly dT, poly dGdC – poly dGdC, (Sigma), calf thymus (ct)-DNA (Aldrich) and dissolved in sodium cacodylate buffer, I = 0.05 M, pH = 7.0. The ct-DNA was additionally sonicated and filtered through a 0.45 mm filter to obtain mostly short (ca. 100 base pairs) rod-like B-helical DNA fragments.[44] Polynucleotide concentration was determined spectroscopically[44] as the concentration of phosphates (corresponds to c (nucleobase)).

Fluorimetric titrations were performed by adding aliquots of nucleotide stock solutions to solution of calixarene ($c = 1 \times 10^{-5}$ M) , using λ_{exc} = 300 nm and monitoring change of emission in whole spectrum, then using change at λ_{em} = 400 nm from calculation of binding constant by fitting to 1:1 stoichiometry of complex formed.

Circular dichroism (CD) spectra were recorded on JASCO J-815 spectropolarimeter at room temperature using 1 cm path quartz cuvettes with a scanning speed of 200 nm/min (an average of three accumulations). A buffer background was subtracted from each spectrum. CD experiments were performed by adding portions of the compound stock solution into the solution of the polynucleotide ($c = 2 \times 10^{-5}$ M).

Thermal melting curves for ds-DNA, ds-RNA, and their complexes with studied compounds were determined as previously described[29] by monitoring the absorption change at 260 nm as a function of temperature. The absorbance of the ligands was subtracted from every curve, and the absorbance scale was normalized. T_m values are the midpoints of the transition curves determined from the maximum of the first derivative and checked graphically by the

tangent method. The ΔT_m values were calculated subtracting T_m of the free nucleic acid from T_m of the complex. Every ΔT_m value here reported was the average of at least two measurements. The error in ΔT_m is $\pm$ 0.5 °C.

Ethidium bromide (EB) displacement assay was done on a Agilent Eclipse fluorimeter in a 1.5 mL of sodium cacodylate buffer in a 1 cm path length quartz cuvette (pH 7.0, I = 0.05 M), excitation at λ = 505 nm and emission at the λ = 600 nm recorded. First, the solution of ethidium bromide (c = 5 × 10^{-6} M) was recorded (Int(EB), subsequently, polynucleotide was added (c = 5 × 10^{-5} M) and emission of EB/polynucleotide was collected (Int(EB/DNA)). Aliquots of tested compound are then gradually added so that the ratio of ethidium bromide to test compound (r = [EB] / [compound]) ranges from 1 to 0.1, and quenching of the EB/DNA complex fluorescence emission was monitored as function of r = [EB] / [compound]. The percentage of EB displaced by compound was calculated, given IDA50% values presenting the ratio r = [EB] / [compound] at which 50% of EB/DNA emission is quenched in respect to emission of free EB (Int(EB)).

DAPI displacement experiment was done on a Jasco J815 CD spectropolarimeter, in a 1.5 mL of sodium cacodylate buffer in a 1 cm path length quartz cuvette (pH 7.0, I = 0.05 M), range 230 – 500 nm, high sensitivity of detector, a scanning speed of 200 nm/min (an average of three accumulations). First, the CD spectrum of AT-DNA solution (c = 2 × 10^{-5} M) was recorded, than DAPI (r[DAPI]/DNA]= 0.6) was added, yielding strong positive ICD band at λ = 375 nm. Gradually, studied compound was added for ratios r = [compd]/[DNA] = 0.2 - 3,2, and CD spectra were collected, monitoring a decrease of the ICD band at 375 nm.[36] The percentage of DAPI displaced by compound was calculated, given IDA50% values presenting the ratio r = [DAPI] / [compound] at which 50% of ICD375nm band is decreased in respect to the zero baseline of the free DNA.

Acknowledgment

Financial support from Croatian Science Foundation (IP-2020-02-3786 and IP-2018-01-5475) is gratefully acknowledged.

Notes and references

1 R. B. Silverman, The Organic Chemistry of Drug Design and Drug Action, Elsevier Academic Press, New York**,** 2004**.**

2 M. Demeunynck, C. Bailly, W. D. Wilson, Small Molecule DNA and RNA Binders: From Synthesis to Nucleic Acid Complexes, Wiley-VCH Verlag GmbH & Co. KGaA, 2004.

3 L. Baldini, A. Casnati, F. Sansone, *Eur. J. Org. Chem.* 2020, **31**, 5056–5069.

4 R. Ludwig, *Microchim. Acta* 2005, **152**, 1–19.

5 V. Bagnacani, V. Franceschi, M. Bassi, M. Lomazzi, G. Donofrio, F. Sansone, A. Casnati, R. Ungaro, *Nat. Commun.* 2013, **4**, 1721.

6 M. Lomazzi, V. Franceschi, V. Bagnacani, C. A. Vezzoni, G. Donofrio, A. Casnati, F. Sansone, *Eur. J. Org. Chem.* 2021, **29**, 1–13.

7 W. B. Hu, C. Blecking, M. Kralj, L. Suman, I. Piantanida, T. Schrader, *Chem. Eur. J.* 2012, **18**, 3589–3597.

8 J. - N. Rebilly, B. Colasson, O. Bistri, D. Over, O. Reinaud, *Chem. Soc. Rev.* 2015, **44**, 467–489.

9 A. Višnjevac, J. Gout, N. Ingert, O. Bistri, O. Reinaud, *Org. Lett.* 2010, **12**, 2044–2047.

10 A. Parrot, S. Collin, G. Bruylants, O. Reinaud, *Chem. Sci.* 2018, **9**, 5479–5487.

11 O. Bistri, O. Reinaud, *Org. Biomol. Chem.* 2015, **13**, 2849–2865.

12 A. Inthasot, N. Le Poul, M. Luhmer, B. Colasson, I. Jabin, O. Reinaud, *Inorg. Chem.* 2018, **57**, 3646–3655.

13 S. Collin, O. Parrot, L. Marcelis, E. Brunetti, I. Jabin, G. Bruylants, K. Bartik, O. Reinaud, *Chem. Eur. J.* 2018, **24**, 17964–17974.

14 O. Bistri, B. Colasson, O. Reinaud, *Chem. Sci.* 2012, **3**, 811–818.

15 A. Maurin, S. Varatharajan, B. Colasson, O. Reinaud, *Org. Lett.* 2014, **16**, 5426–5429.

16 M. Dhaenens, J. - M. Lehn, J. - P. Vigeron, *J. Chem. Soc. Perkin Trans.* 1993, **2**, 1379–1381.

17 H. Y. Kuchelmeister, C. Schmuck, *Chem. Eur. J*. 2011, **17**, 5311–5318.

18 I. Piantanida, B. S. Palm, P. Cudic, M. Zinic, H. J. Schneider, *Tetrahedron* 2004, **60**, 6225–6231.

19 I. Piantanida, B. S. Palm, P. Cudic, M. Zinic, H. J. Schneider, *Tet. Lett.* 2001, **42**, 6779–6783.

20 D. Ghosh, S. Rhodes, K. Hawkins, D. Winder, A. Atkinson, W. Ming, C. Padgett, J. Orvis, K. Aiken, S. Landge, *New J. Chem.* 2015, **39**, 295–303.

21 C. Remy, H. Guyon, J. N. Rebilly, I. Leray, O. Reinaud, *Chemistry* 2017, **23**, 8669–8677.

22 S. Grimme, J. Antony, S. Ehrlich, H. Krieg, *J. Chem. Phys.* 2010, **132**, 154104–154119.

23 M. Tranfić Bakić, K. Leko, N. Cindro, T. Portada, T. Hrenar, L. Frkanec, G. Horvat, J. Požar, V. Tomišić, *Croat. Chem. Acta* 2017, **90**, 711–725.

24 M. J. Frisch, G. W. Trucks, H. B. Schlegel, G. E. Scuseria, M. A. Robb, J. R. Cheeseman, G. Scalmani, V. Barone, B. Mennucci, G. A. Petersson, H. Nakatsuji, M. Caricato, X. Li, H. P. Hratchian, A. F. Izmaylov, J. Bloino, G. Zheng, J. L. Sonnenberg, M. Hada, M. Ehara, K. Toyota, R. Fukuda, J. Hasegawa, M. Ishida, T. Nakajima, Y. Honda, O. Kitao, H. Nakai, T. Vreven, J. A. Montgomery, Jr., J. E. Peralta, F. Ogliaro, M. Bearpark, J. J. Heyd, E. Brothers, K. N. Kudin, V. N. Staroverov, R. Kobayashi, J. Normand, K. Raghavachari, A. Rendell, J. C. Burant, S. S. Iyengar, J. Tomasi, M. Cossi, N. Rega, J. M. Millam, M. Klene, J. E. Knox, J. B. Cross, V. Bakken, C. Adamo, J. Jaramillo, R. Gomperts, R. E. Stratmann, O. Yazyev, A. J. Austin, R. Cammi, C. Pomelli, J. W. Ochterski, R. L. Martin, K. Morokuma, V. G. Zakrzewski, G. A. Voth, P. Salvador, J. J. Dannenberg, S. Dapprich, A. D. Daniels, Ö. Farkas, J. B. Foresman, J. V. Ortiz, J. Cioslowski, D. J. Fox, Gaussian, Inc., Wallingford CT, 2016.

25 C. Yuan, X. Y. Wu, L. Lu, M. Zhu, *Spectrochim. Acta A Mol. Biomol. Spectrosc.* 2016, **154**, 215–219.

26 J. Liu, X. Meng, H. Duan, T. Xu, Z. Ding, Y. Liu, L. Lucia, *Sensors and Actuators B*, 2016, **227**, 296–303.

27 H. Gampp, M. Maeder, C. J. Meyer, A. D. Zuberbuhler, *Talanta* 1985, **32**, 257–264.

28 M. Maeder, A. D. Zuberbuehler, *Anal. Chem*., 1990, **62**, 2220–2224.

29 J. L. Mergny, L. Lacroix, *Oligonucleotides* 2003, **13**, 515–537.

30 E. Garcia-España, I. Piantanida, H. J. Schneider, Nucleic Acids as Supramolecular Targets, Royal Society of Chemistry, London, 2013.

31 A. C. Sedgwick, J. T. Brewster, T. H. Wu, X. Feng, S. D. Bull, X. H. Qian, J. L. Sessler, T. D. James, E. V. Anslyn, X. L. Sun, *Chem. Soc. Rev.* 2021, **50**, 9–38.

32 R. Palchaudhuri, P. U. Hergenrother, *Curr. Opin. Biotechnol.* 2007, **18**, 497–503.

33 W. C. Tse, D. L. Boger, *Acc. Chem. Res*. 2004, **37**, 61–69.

34 M. Eriksson, B. Nordén, *Methods in Enzymology*, 2001, **340**, 68–98.

35 T. Šmidlehner, I. Piantanida, G. Pescitelli, *Beilstein J. Org. Chem.* 2018, **14**, 84–105.

36 N. H. List, J. Knoops, J. Rubio-Magnieto, J. Ide, D. Beljonne, P. Norman, M. Surin, M. Linares, *J. Am. Chem. Soc.* 2017, **139**, 14947–14953.
37 D. Coquière, J. Marrot, O. Reinaud, *Chem. Commun*. 2006, 3924–3926.
38 S. Grimme, J. Antony, S. Ehrlich, H. Krieg, *J. Chem. Phys*. 2010, **132**, 154104–154119.
39 M. Tranfić Bakić, K. Leko, N. Cindro, T. Portada, T. Hrenar, L. Frkanec, G. Horvat, J. Požar, V. Tomišić, *Croat. Chem. Acta* 2017, **90**, 711–725.
40 S. Grimme, C. Bannwarth, P. Shushkov, *J. Chem. Theory Comput.* 2017, **9**, 1989–2009.
41 C. Bannwarth, S. Ehlert, S. Grimme, *J. Chem. Theory Comput.* 2019, **12**, 1652–1671.
42 C. Bannwarth, E. Caldeweyher, S. Ehlert, A. Hansen, P. Pracht, J. Seibert, S. Spicher, S. Grimme, *WIREs Comput. Mol. Sci.* 2020, **11**, e01493.
43 ChemSpider. Available online: http://www.chemspider.com/Chemical-Structure.5858.html and https://www.chemspider.com/Chemical-Structure.5901.html, respectively. Accessed on 19th July, 2021.
44 K. Ester, M. Hranjec, I. Piantanida, I. Caleta, I. Jarak, K. Pavelic, M. Kralj, G. Karminski-Zamola, *J. Med. Chem.* 2009, **52**, 2482–2492.